# Effect of aging on functional brain networks: a graph-theoretical analysis

**Lubica Benuskova[1], Paul McCarthy[2], Elizabeth A. Franz[3]**

[1]Department of Applied Informatics, FMFI, Comenius University, Bratislava, Slovakia
[2]Department of Computer Science, University of Otago, Dunedin, New Zealand
[3]Department of Psychology, University of Otago, Dunedin, New Zealand
Email: lubica@ii.fmph.uniba.sk

## Abstract

Graph theory is a novel approach to the analysis of functional connectivity in the brain. We have performed graph theoretical analysis of an fMRI data set from a study conducted in 2000 by Buckner et. al. Buckner et al. (2000), in an attempt to find differences between healthy participants, both young and aged, and aged participants with mild Alzheimer's Disease. We apply our techniques to the data, and also give a preliminary statistical comparison across these groups. Our results show that there are statistically significant differences between the groups in several global network characteristics, including density, number of nodes and maximum degree. We hypothesise that these differences reflect a general change in how the aging brain copes with everyday tasks, meaning an increased effort required by aged brains to perform, which is further accentuated by the onset of Alzheimer's disease.

## 1 Introduction

The human brain is an incredibly complex system, consisting of billions of neurons, interacting over trillions of synaptic connections. These interactions give us consciousness and intelligence, control our core functions, and allow us to manipulate our environment. Functional magnetic resonance imaging, or fMRI, allows us to measure neural activity throughout the brain over time. From these measurements, we may gain insights into the functional connectivity of the brain, i.e. how different parts interact with each other when the brain is solving a particular task or just when it is idle. How can we analyse these interactions, and how do they change with age and onset of Alzheimer's disease? This paper attempts to address these questions by using graph theory techniques to analyse functional connectivity derived from fMRI data.

Alzheimer's disease (AD) is the most common form of dementia, causing progressive cognitive decline, with age the primary risk factor (Gauthier (2007)). The pathology of AD is characterised by extracellular deposits of senile, or amyloid plaques, mainly in the cerebral, cortical and hippocampal regions, and neurofibrillary tangles that occupy much of the cytoplasm of neurons. In addition, brains from AD patients demonstrate degenerative changes, inflammation as well as neuronal cell loss and synaptic dysfunction, which have been assumed to be consequences of the accumulation of pathological protein components (Gauthier (2007)). Aging by itself causes changes in the brains of healthy people. Global volume of grey matter, i.e. number of neurons, decreases with age, although the effect is not uniformly distributed throughout the brain. It is interesting that global white matter, i.e. number of myelinated axons, does not decline with age, but local areas of relative loss and relative preservation exist.

Functional Magnetic Resonance Imaging, or fMRI, is a technique for capturing high resolution 3D images of oxygenated blood levels in the brain. fMRI measures the ratio of oxygenated to de-oxygenated blood throughout the brain; this ratio is referred to as the Blood Oxygen Level Dependent (BOLD) contrast Ogawa et al. (1992). Evidence suggests that, as neural activity in a brain region increases, a corresponding increase in blood flow to that region occurs, bringing in oxygen to fuel the increased rate of metabolism. Thus, neural activity throughout the brain may be inferred from the subsequent change in the BOLD contrast Ulmer & Jansen (2010); Buxton (2009). A typical fMRI image consists of 3D pixels, known as *voxels*, each representing an area as small as $\sim 1mm^3$.

Graph theory has become a popular approach for the analysis of fMRI data (see e.g. Sporns et al. (2004); Bullmore & Sporns (2009); Rubinov & Sporns (2010)). Graph theoretical analysis can provide insights into neural behaviour not readily achievable using more traditional approaches, such as principal component analysis (PCA) Friston et al. (1993), and statistical parametric mapping (SPM) Friston et al. (1990). Friston et. al. Friston et al. (1993) formalised definitions for the three forms of connectivity most commonly of interest: *functional connectivity*, temporal correlation between neural events occurring in spatially distinct brain regions; *effective connectivity*, the influence that one brain region exerts upon another; and *anatomical connectivity*, the physical connections which exist between brain regions. fMRI is an ideal technique for deriving functional and effective connectivity; while anatomical connectivity may be measured using more advanced tech-

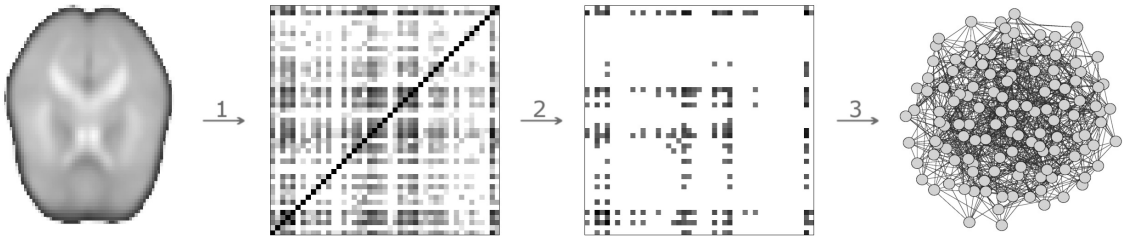


Obr. 1: The process of creating a graph from an fMRI data set proceeds as follows: **1.** Temporal correlation values are calculated between the time series data for every pair of voxels, creating a square symmetric correlation matrix. **2.** This matrix is thresholded to remove low correlation values. **3.** The matrix is then converted into a simple undirected, unweighted graph, where nodes represent voxels, and edges represent strong temporal correlation between pairs of voxels.

nologies such as diffusion spectrum or tensor imaging (e.g. Hagmann et al. (2007)), or using statistical methods on MRI data (e.g. He et al. (2007)).

Graphs are an intuitively appealing structure for use in the analysis of functional connectivity: regions of the brain are represented in a graph as nodes, and interaction between regions as edges. A directed graph may be used to model effective connectivity (i.e. causal, or influential relationships between brain regions), and edge weights may be used to represent the strength of inter-regional relationships. In this study however, we have worked only with undirected, unweighted graphs, and are thus assuming that relationships between nodes are symmetrical. The procedure followed in this study is described in Figure 1.

Interpreting the results provided by graph theoretical analysis is a non-trivial task. Rubinov and Sporns Rubinov & Sporns (2010) give an excellent overview of current trends in the interpretation of the various measures that may be calculated upon graphs generated from brain imaging data. These range from simple measures, such as node degree, to more complex high level measures, such as modularity Newman & Girvan (2004) and betweenness centrality Freeman (1979). In this short paper, we will limit our discussion to those measures that are easily interpretable and useful for making inferences about aged related changes in the functional connectivity of the brain; we focus on global differences between the graphs under analysis.

## 2 Data and Methods

### 2.1 The data

Structural and functional MRI data, from a study conducted by Buckner et. al. in 2000, were used as a basis for our analysis (Buckner et al. (2000); http://www.fmridc.org). Data were acquired from 41 participants: fourteen participants were categorised as 'young' (mean age 21.1, S.D. 2.0), fifteen as 'aged' (mean age 75.1, S.D. 6.9), and the remaining twelve (mean age 77.1, S.D. 5.3) as 'aged with Alzheimer's Disease (AD)', having very mild to mild Dementia of the Alzheimer Type according to the Clinical Dementia Rating (CDR) Morris (1997). Seven participants in the aged with AD group had CDR scores of 0.5 (very mild), and the remaining five had CDR scores of 1.0 (mild). There was no statistically significant difference in age between the means of the aged and aged with AD group, as assessed by a two-tailed independent sample $t$-test ($p = 0.58$).

The study involved participants completing a simple visual-motor task, in an event based experimental paradigm Friston et al. (1998). Each participant underwent four fMRI recording sessions, referred to as *runs*. Each run consisted of 128 fMRI images, with a TR (image acquisition) time of 2.68 seconds. During a single run, 15 *trials* were executed, each having a duration of 8 images (21.44 seconds), making a total recording time of approximately 5.5 minutes per run (the first trial in each run began at image #5, and the last trial ended at image #125). A trial consisted of either one or two visual stimuli, presented as a flickering checkerboard pattern; the participants were instructed to push a button with their right index finger upon onset of each stimulus. During a 'one-stimulus' trial, the stimulus was triggered at the start of the trial. During a 'two-stimulus' trial, the first stimulus was triggered at the start of the trial, and the second stimulus was triggered 5.36 seconds after the first. One- and two-stimulus trials were pseudorandomly inter-mixed.

### 2.2 Data preprocessing

Data preprocessing consisted of the steps described below. Before any preprocessing, the first four and last four images from every run were discarded, as they were not part of any trial.

1. *Visual inspection*: Every run in the raw data was visually inspected to check for obvious anomalies. This step uncovered three suspect data sets; the data for participant #3 were discarded, due to the

presence of significant noise throughout every run. The data for participants #15 and #19 contained aliasing effects, which were manually corrected. These three data sets were from the aged group; a two-tailed independent sample $t$-test revealed no age difference between means of the aged and aged with AD group after the removal of participant #3.

2. *Slice-timing correction*: The fMRI slices were captured in an interleaved manner, thus every run was corrected for slice timing differences using Fourier interpolation; this was accomplished with the `3dTshift` tool, provided with AFNI[1] (Cox (2011)).

3. *High-pass temporal filtering*: To correct for scanner drift, and to remove long term trends, a high-pass temporal filter was applied to every run, with a pass frequency of $1/42.88 \sim 0.02Hertz$ (the duration of two trials). This was achieved using the `fslmaths` utility, provided with FSL[2] (Smith et al. (2004)).

4. *Motion correction*: Motion correction was performed using a 6-parameter rigid body transformation. For each run, a mean image was created; every image within the run was then aligned to this mean image. AIR[3] was used for motion correction, and for all subsequent image alignment steps Woods et al. (1992).

5. *Brain segmentation*: Non-brain matter was removed from each participant's structural MRI image, using the `bse` utility provided with BrainSuite[4] Shattuck & Leahy (2002); Shattuck et al. (2001).

6. *Intra-participant registration*: For every run, a mean fMRI image was created, and aligned to the corresponding structural MRI image using a 12-parameter affine transformation. The alignment parameters were then applied to each image in the run, to bring them into alignment.

7. *Spatial normalisation*: Every image was then aligned to the ICBM452 atlas (Mazziotta et al. (2001)). This was accomplished in two steps: first, the participant's structural MRI image was aligned to the atlas using a non-linear 60 parameter transformation; then, the same alignment parameters were applied to the participant's fMRI images. This two step method is considered to achieve better results than aligning fMRI images directly to the atlas (Filippi (2009); Strother (2006)). Finally, the fMRI images were resampled back to the original resolution of $64\times64\times16$ voxels.

For each participant, all 60 trial periods were averaged to create one fMRI volume, 21.44 seconds (8 images) in duration; all trials were included in these averages, as it was considered unnecessary to distinguish between 'one-stimulus' and 'two-stimulus' trials Dale & Buckner (1997). Graph theoretical analysis was then applied to these volumes.

### 2.3 Graph creation

Undirected and unweighted graphs were created from the fMRI data for every participant (see Figure 1). All voxels that exceeded a BOLD level of 200 at any point in time were included as nodes in each graph. The threshold value of 200 was selected after an analysis of the BOLD intensity distribution for each group, as shown in Figure 2. The values below 200 represent non-neural artifacts. Pearson's Correlation Coefficient $r$ (Rodgers & Nicewander (1988)) was calculated between the time series data for all pairs of nodes $x$ and $y$ (Eguiluz et al. (2005)):

$$r(x,y) = \frac{\sum(x_i - \overline{x})\,(y_i - \overline{y})}{\sqrt{\sum(x_i - \overline{x})^2\ \sum(y_i - \overline{y})^2}} \qquad (1)$$

where $x_i$ and $y_i$ is the activity in voxels $x$ and $y$ at time $i$, respectively, and $\overline{x}$ and $\overline{y}$ are the means of the time series data for voxels $x$ and $y$ respectively.

Three graphs for each participant were created from the correlation matrices, using correlation thresholds $r_c$ of 0.8, 0.9 and 0.95. Edges were added between nodes with an absolute correlation value greater than or equal to the threshold; both positive and negative correlations were included to account for excitatory and inhibitory relationships between nodes. Disconnected nodes (nodes which exceeded the BOLD threshold, but were not strongly correlated with any other nodes in the graph), and small components (components less than 20 nodes in size) were removed before further analysis, to prevent skewing of global graph measures. For every graph generated, the remaining nodes formed a single connected component.

### 2.4 Graph analysis

Standard measures of these undirected, unweighted graphs were calculated, including number of nodes, degree $k$, density $d$, degree distribution $P(k)$, maximum degree, characteristic path length $L$, clustering coefficient $C$, small-world index, assortativity and global efficiency. The *degree* $k$ of a node is simply the number of neighbours of that node (Diestel (2005)). The *clustering coefficient* $C$ is the ratio of the number of edges which are present between a node's neighbours to the number of possible edges (Watts & Strogatz (1998)). In other

[1] `http://afni.nimh.nih.gov/afni`
[2] `http://www.fmrib.ox.ac.uk/fsl/`
[3] `http://bishopw.loni.ucla.edu/air5/`
[4] `http://users.loni.ucla.edu/~shattuck/brainsuite/`

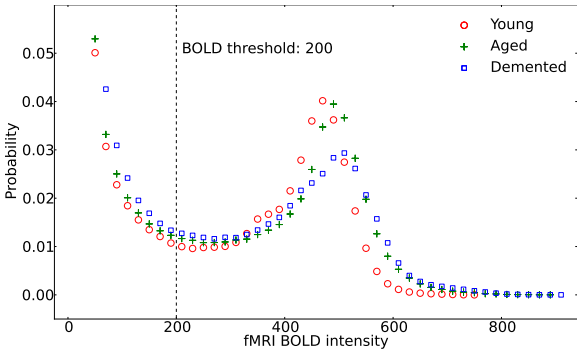


Obr. 2: fMRI BOLD intensity distribution for the young, aged, and aged with AD data sets. A BOLD value of 200 was chosen as the threshold for inclusion of voxels as nodes in the graphs.

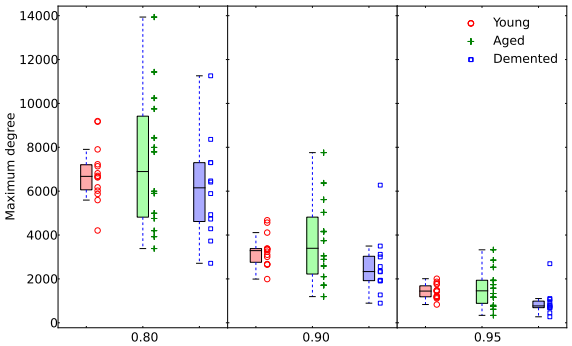


Obr. 3: Maximum node degree for the three groups and three correlation thresholds. The mean of aged with AD graphs is significantly lower than young and aged graphs at $r_c = 0.95$ ($p < 0.05$).

words, the clustering coefficient of a node is the density of the subgraph formed by the node's immediate neighbours, and the edges which exist between them. The *density* is the average ratio of true edges to the maximum possible number of edges from each node in the graph. The *characteristic path length* $L$ is the average shortest path length between all pairs of nodes in a graph (Watts & Strogatz (1998)).

The degree distribution $P(k)$ of a graph is the probability distribution of a node in the graph having degree $k$. A random graph[5] (P. Erdős (1960)) has a Gaussian degree distribution, with the peak equal to the average node degree. A *scale-free* network, on the other hand, has a power law degree distribution, i.e. $P(k) \sim k^{-\gamma}$, where $\gamma$ is the power law scaling exponent (Barabasi & Albert (1999)). Scale-free simply means that degrees are not grouped around a single value (peak), or scale, but instead are spread over a wide range of values that can span several orders of magnitude. This implies a potentially rich internal structure, and suggests the presence of highly connected *hubs* in the graph. The maximum degree of a graph therefore gives us the size of the largest hub.

*Small-world* networks are characterised by a high level of clustering, i.e. $C \gg C_{random}$, combined with a low characteristic path length, i.e. $L \approx L_{random}$ (Watts & Strogatz (1998)). A small-world network is typically portrayed as consisting of densely connected clusters of nodes, with long range connections between clusters. The small-world index (Humphries et al. (2006)) is therefore a combination of two ratios, $\frac{\gamma}{\lambda}$, where $\gamma = \frac{C}{C_{random}}$, and $\lambda = \frac{L}{L_{random}}$. The clustering coefficient of a random graph with number of nodes $n$ and density $d$ is equal to $d$, and the characteristic path length may be approximated by $\frac{\ln n - 0.5772}{\ln d(n-1)} + \frac{1}{2}$ (Agata Fronczak (2004)). This ratio is used as a measure of 'small-worldness': a graph with a small-world index greater than 1 is considered to have small-world characteristics.

[5]More specifically, an Erdős-Rényi random graph.

*Assortativity* (Newman (2002)) is a measure of the probability that nodes in a graph are connected to other nodes of similar degree. A graph with a high assortativity indicates that nodes will tend to connect to other nodes which have a similar degree, whereas nodes in a graph with a low (negative) assortativity tend to be connected to nodes with a different degree. *Efficiency* (Vito Latora (2001)) is a measure of information flow through a graph; the global efficiency of a graph is calculated as the average inverse of shortest path lengths between all pairs of nodes. Latora and Marchiori Vito Latora (2001) suggest the use of efficiency as an alternative to the small-world index, to measure the small-world nature of a graph.

## 3 Results

Group averaged graph measures are provided in Table 1. A two-sample statistical analysis was performed between each pair of groups; Levene's test was used to test for equality of variance, and two-tailed independent sample *t*-tests (for equal or unequal variances, depending upon the outcome of the Levene's test) were used to test for differences in means, between the three groups. Some interesting results emerge from the figures in Table 1. The main differences which are statistically significant:

- Young graphs have less nodes than both aged and aged with AD graphs (less voxels with a BOLD intensity $\geq 200$), significant at $p < 0.001$ for all correlation thresholds. The BOLD intensity distributions in Figure 2 support this: aged and aged with AD participants seem to have more voxels at high intensities than young participants.

- Young graphs have less disconnected nodes (nodes which have no correlation with other nodes) than both aged and aged with AD graphs at $r_c = 0.9$. However, for $r_c = 0.95$ the relationship is reversed:

Tab. 1: Mean (standard deviation in brackets) graph measures for the three groups, at each correlation threshold.

| | Young | | Aged | | Aged with AD | |
|---|---|---|---|---|---|---|
| **Correlation threshold 0.8** | | | | | | |
| *Disconnected nodes*[a] | 0.0 | (0.0) | 0.0 | (0.0) | 0.0 | (0.0) |
| *Nodes* | 22888.6$^{***\S\S\S}$ | (996.1) | 24750.1$^{***}$ | (1287.9) | 24298.8$^{\S\S\S}$ | (864.0) |
| *Density* | 0.0937 | (0.0302)$^{**}$ | 0.1064 | (0.0604)$^{**}$ | 0.0813 | (0.0406) |
| *Degree* | 2132.65 | (662.65)$^{**}$ | 2618.53 | (1502.60)$^{**}$ | 1972.83 | (987.07) |
| *Maximum degree* | 6806.43 | (1328.60)$^{**}$ | 7337.86 | (3157.08)$^{**}$ | 6114.42 | (2306.98) |
| *Path length* | 2.3620 | (0.0853)$^{**}$ | 2.3336 | (0.1606)$^{**}$ | 2.3824 | (0.1108) |
| *Clustering coefficient* | 0.5012 | (0.0435)$^{**}$ | 0.5135 | (0.0826)$^{**}$ | 0.4823 | (0.0608) |
| *Small-world index* | 4.2068 | (0.9202)$^{**}$ | 4.5307 | (1.8788)$^{**}$ | 5.0475 | (1.5562) |
| *Assortativity* | 0.5371 | (0.0749) | 0.5273 | (0.1215) | 0.5440 | (0.0690) |
| *Global efficiency* | 0.4709 | (0.0242)$^{**}$ | 0.4799 | (0.0469)$^{**}$ | 0.4634 | (0.0318) |
| **Correlation threshold 0.9** | | | | | | |
| *Disconnected nodes*[a] | 1.50$^{**\S}$ | (3.37)$^{**\S}$ | 5.57$^{**}$ | (4.65)$^{**}$ | 5.67$^{\S}$ | (6.02)$^{\S}$ |
| *Nodes* | 22887.1$^{***\S\S\S}$ | (995.9) | 24744.6$^{***}$ | (1289.4) | 24293.1$^{\S\S\S}$ | (867.4) |
| *Density* | 0.0263 | (0.0109)$^{*}$ | 0.0316 | (0.0225)$^{*}$ | 0.0206 | (0.0157) |
| *Degree* | 597.45 | (241.11)$^{**}$ | 775.40 | (561.58)$^{**}$ | 499.64 | (383.06) |
| *Maximum degree* | 3294.36 | (745.07)$^{**\S}$ | 3720.36 | (1931.91)$^{**}$ | 2588.33 | (1379.51)$^{\S}$ |
| *Path length* | 3.4689 | (0.1582)$^{**\S}$ | 3.3869 | (0.2913)$^{**}$ | 3.4713 | (0.2090)$^{\S}$ |
| *Clustering coefficient* | 0.4253 | (0.0332)$^{**}$ | 0.4355 | (0.0629)$^{**}$ | 0.4119 | (0.0448) |
| *Small-world index* | 10.50$^{\S}$ | (3.47)$^{***}$ | 12.99 | (8.45)$^{***}$ | 16.08$^{\S}$ | (7.67) |
| *Assortativity* | 0.5969 | (0.0657)$^{*}$ | 0.5901 | (0.1120)$^{*\dagger}$ | 0.6275 | (0.0692)$^{\dagger}$ |
| *Global efficiency* | 0.3279 | (0.0207)$^{**}$ | 0.3404 | (0.0414)$^{**}$ | 0.3252 | (0.0292) |
| **Correlation threshold 0.95** | | | | | | |
| *Disconnected nodes*[a] | 764.79$^{*\S\S}$ | (126.62) | 647.86$^{*}$ | (118.03) | 629.83$^{\S\S}$ | (133.20) |
| *Nodes* | 22123.8$^{***\S\S\S}$ | (1084.8) | 24102.3$^{***}$ | (1333.3) | 23668.9$^{\S\S\S}$ | (836.6) |
| *Density* | 0.0069 | (0.0032)$^{*}$ | 0.0081 | (0.0064)$^{*}$ | 0.0047 | (0.0046) |
| *Degree* | 151.20 | (67.58)$^{**}$ | 194.34 | (155.53)$^{**}$ | 110.15 | (109.57) |
| *Maximum degree* | 1425.79$^{\S\S}$ | (336.23)$^{**}$ | 1575.58$^{\dagger}$ | (879.49)$^{**}$ | 916.75$^{\S\S\dagger}$ | (606.22) |
| *Path length* | 5.7920 | (0.4651)$^{**}$ | 5.5162 | (0.7766)$^{**}$ | 5.6872 | (0.5816) |
| *Clustering coefficient* | 0.3933 | (0.0220)$^{**}$ | 0.3917 | (0.0425)$^{**}$ | 0.3787 | (0.0327) |
| *Small-world index* | 28.12$^{\S}$ | (11.87)$^{***\S}$ | 43.27 | (37.10)$^{***}$ | 60.18$^{\S}$ | (38.09)$^{\S}$ |
| *Assortativity* | 0.6555$^{\S}$ | (0.0495)$^{*}$ | 0.6504 | (0.0849)$^{*}$ | 0.7035$^{\S}$ | (0.0654) |
| *Global efficiency* | 0.2100 | (0.0221)$^{**}$ | 0.2196 | (0.0399)$^{**}$ | 0.2064 | (0.0284) |

[a] These values include both disconnected nodes and components less than 20 nodes in size. These nodes were removed before any further processing.

$^{*}$ Significantly different between young and aged ($^{*}$ $p < 0.05$, $^{**}$ $p < 0.015$, $^{***}$ $p < 0.001$).

$^{\S}$ Significantly different between young and aged with AD ($\S$ $p < 0.05$, $\S\S$ $p < 0.015$, $\S\S\S$ $p < 0.001$).

$^{\dagger}$ Significantly different between aged and aged with AD ($\dagger$ $p < 0.05$, $\dagger\dagger$ $p < 0.015$, $\dagger\dagger\dagger$ $p < 0.001$).

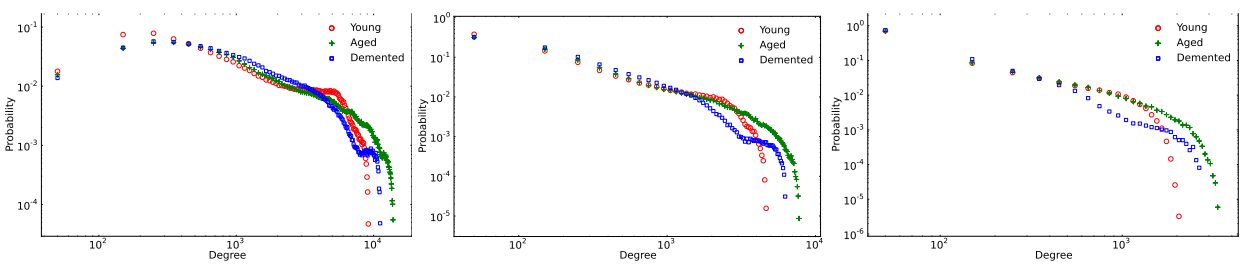


(a) Correlation threshold 0.8 (b) Correlation threshold 0.9 (c) Correlation threshold 0.95

Obr. 4: Accumulated degree distribution for the three groups at each correlation threshold.

young graphs have more disconnected nodes than both aged and aged with AD graphs at the higher threshold.

- Aged with AD graphs have a greater small-world index than young graphs, significant at $p < 0.05$ for $r_c \geq 0.9$.
- The only difference between the aged and aged with AD groups is the maximum degree at correlation threshold $r_c$ = 0.95: aged with AD graphs have a lower maximum degree than both young and aged graphs. By looking at the boxplot (Figure 3), we can see that this trend exists at the other thresholds, but is only statistically significant at $r_c$ = 0.95.
- Assortativity of the aged with AD graphs is higher than in the young graphs ($p < 0.05$), at $r_c = 0.95$.
- Variances of almost all topological characteristics are significantly higher for aged graphs, when compared to young graphs. There are less differences in variance between the young and aged with AD graphs.

# 4 Discussion

## 4.1 AD, but not age, leads to reduced functional connectivity

Despite no significant difference in average degree or density between any of the three groups, aged with AD graphs have a lower maximum degree than both young and aged graphs at correlation threshold $r_c = 0.95$. This seems to contradict the trend portrayed by the accumulated degree distributions, shown in Figure 4. However, further exploration reveals that the aged with AD data are heavily skewed by a single graph with a much greater density - denser than any other graph in the group by a factor of at least 1.6 at $r_c = 0.8$, and at least 2.2 at $r_c \geq 0.9$. This same outlier is evident in Figure 3, for $r_c \geq 0.9$. Figure 5 displays the accumulated degree distribution for $r_c = 0.95$, with this outlier graph removed. In fact, by removing this graph from the data set, and repeating the two-tailed independent sample $t$-tests, we find that the aged with AD group has significantly lower density, degree and maximum degree than both the young and aged groups, for $r_c \geq 0.9$, as shown in Table 2. The removed subject had a CDR score of 0.5, it is plausible that this was a case of misdiagnosis.

Pathologically, these results make more sense: the neuronal and synaptic atrophy which is known to occur in AD should have a marked impact on the functional connectivity of the brain. These findings are also consistent with other studies on the effects of AD on functional connectivity: Leuchter et. al. Leuchter et al. (1992) found consistently reduced coherence at all frequency bands, in AD subjects, using EEG; Greicius et. al. Greicius et al. (2004), working with the data set from Buckner et. al.'s study Buckner et al. (2000) (the same data set that was used in this study), found disrupted connectivity around the posterior cingulate and hippocamupus in the aged with AD group, using independent component analysis (ICA) (Beckmann & Smith (2004); Sorg et. al. Sorg et al. (2007)) found reduced functional connectivity between the hippocampus and temporal lobe, in subjects at risk of developing AD, using ICA on resting-state fMRI data; Wang et. al. Wang et al. (2007) found reduced inter-lobe connectivity patterns, but increased intra-lobe connectivity, in early AD patients, by calculating and comparing correlation coefficients between all pairs of regions; Supekar et. al. (Supekar et al. (2008)) reported reduced regional connectivity in resting-state fMRI data acquired from AD patients, using wavelet analysis and graph theory.

The increased connectivity present in the aged group relative to the young group, clearly visible in the degree distribution plots (Figures 4 and 5) is a matter of some interest; this difference is still present when the degree values are normalised by graph size, to degree centrality (Freeman (1979)). It is known that the distribution of neural metabolism throughout the brain changes with age, giving credence to the idea that we develop compensatory and adaptive mechanisms to overcome the pathological changes associated with aging. However, studies to date on the functional connectivity of aging (e.g. Greicius et al. (2004); Stam et al. (2007, 2009); de Haan et al. (2009); Buckner et al. (2009)) have found reduced, or non-uniform changes in the functional connectivity of aged subjects, when compared with young subjects. This discrepancy may be caused by the reduced signal-to-noise ratio in fMRI BOLD signals from aged brains (van den Heuvel et al. (2009)); an effect which could also explain the higher variances exhibited in the aged group for many of the network measures. Comparison between these studies is somewhat difficult, due to methodological differences, however, the increased functional connectivity and neural metabolism in the aged group, observed in this study, supports our hypothesis that aged brains have to work harder to perform; this is discussed further in the next section.

## 4.2 Aged brains work harder

Young graphs have less nodes than both aged and aged with AD graphs (i.e. less voxels with a BOLD intensity $\geq 200$), significant at $p < 0.001$. An increased BOLD signal means an increase in oxygenated blood flow, which implies increased neural metabolism. Therefore this finding may mean that the aged and aged with AD participants had to work harder than the young participants to perform the task. This finding is in agreement with findings of increased frontal activation in aged

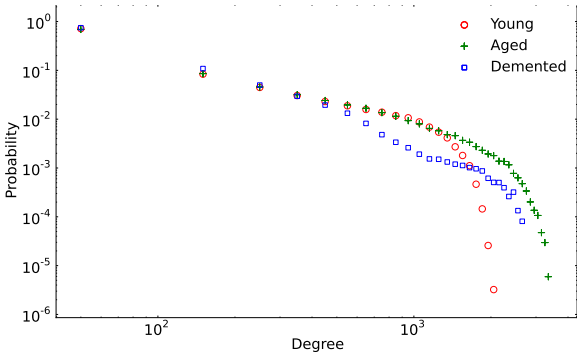


Obr. 5: Accumulated degree distribution for the three groups, at correlation threshold $r_c = 0.95$. A single outlier graph has been removed from the aged with AD group, dramatically affecting the distribution.

brains (He et al. (2008); de Haan et al. (2009); Buckner et al. (2009)). An alternate or additional explanation is skewing of the BOLD distribution by increased ventricular, and hence cerebrospinal fluid volume, in the aged and aged with AD groups (Buckner et al. (2009)).

We found opposing trends for disconnected nodes at correlation thresholds 0.9 and 0.95. For $r_c = 0.9$, young graphs had less disconnected nodes than both aged and aged with AD graphs. That is, less nodes in the aged and aged with AD graphs than in the young graphs were functionally connected with any other nodes at a correlation of 0.9. The total number of disconnected nodes in each group, however, was less than 0.001% of the total number of nodes. For $r_c = 0.95$, young graphs had more disconnected nodes than both aged and aged with AD graphs. The total number of disconnected nodes in each group at $r_c = 0.95$ was again quite small, at around 5%, so this could be considered to be nothing more than noise.

### 4.3 Strong small-world characteristics

An interesting finding was that aged with AD graphs have a larger small-world index than young graphs for thresholds $r_c \geq 0.9$ (this difference was still significant at $p < 0.05$ after removal of the outlier from the aged with AD group at both correlation thresholds[6]). There was no significant difference between the aged and aged with AD groups, possibly due to the large variances in these two groups. All three groups exhibit extremely high clustering when compared to random graphs of the same density. In particular, despite having lower densities, the aged with AD graphs maintain their level of clustering at the high correlation threshold of 0.95. The high clustering in each group is enough to overwhelm the fact that, at all correlation thresholds, the characteristic path length is higher than that of an equivalent random graph.

This finding is in contrast to a number of studies (e.g. Stam et al. (2007, 2009); Supekar et al. (2008); de Haan et al. (2009)), which all found decreased clustering and increased path length in AD subjects, and a corresponding reduction in the small-world index. However, these studies are not directly comparable due to methodological differences. A common approach in graph theoretical analysis is to vary the correlation (or analagous measure) threshold for each graph, ensuring that all graphs to be compared are of similar densities. Our approach is different, in that by using the same threshold for each group, we are comparing graphs of varying densities, but at the *same level of functional connectivity*; we feel this is an important characteristic to retain, when comparing across groups. Furthermore, as no differences were found between the three groups in clustering or path length, we argue that the difference in magnitude of the small-world index (which is wholly derived from these parameters and graph density) primarily reflects the difference in densities between the graphs. This does not discount the fact that all graphs in the study show a strong small-world structure and internal clustering, which implies the presence of a very strong modular structure, and alone warrants further regional analysis of the data.

The accumulated degree distributions shown in Figures 4 and 5 closely resemble that of a decaying, or truncated power-law, as described by Amaral et. al. Amaral et al. (2000), and reported in a number of other studies on functional connectivity (e.g. Eguiluz et al. (2005); Bassett & Bullmore (2006); Achard et al. (2006)). This lends weight to the idea that the 'preferential attachment' model Barabasi & Albert (1999) is not suitable for modelling real world biological networks; once a node reaches a certain connectivity, there is a *physical cost* associated with acquiring more links Achard et al. (2006); Bullmore & Sporns (2009). Buckner et. al. Buckner et al. (2009) found that high-degree hubs in the cerebral cortex are more likely to be affected by amyloid deposition than their low-degree counterparts, giving a plausible explanation for the lower connectivity exhibited by the aged with AD group (after removal of the dense outlier graph).

## 5 Conclusion

A potentially revealing finding is the fewer nodes found in the young controls compared to the older groups. This points to age as a mediating factor in the work required to perform the task, a possibility that is corroborated by our findings on the increased functional connectivity in aged brains. There was strong evidence of small-worldness in all groups, and particularly high clustering even in the aged with AD group, suggesting the presence of a highly modular structure. Re-

[6] This outlier is not the same subject as the dense outlier previously discussed.

Tab. 2: Mean (standard deviation in brackets) graph measures, after removal of the outlier graph from the aged with AD group.

| | Aged with AD | |
|---|---|---|
| **Correlation threshold 0.9** | | |
| *Density* | $0.0165^{\S\dagger}$ | $(0.0072)^{\dagger\dagger}$ |
| *Degree* | $398.90^{\S\dagger}$ | $(165.72)^{\dagger\dagger}$ |
| *Maximum degree* | $2253.27^{\S\S\dagger}$ | $(781.96)^{\dagger\dagger}$ |
| **Correlation threshold 0.95** | | |
| *Density* | $0.0034^{\S\S\dagger}$ | $(0.0017)^{\dagger\dagger}$ |
| *Degree* | $80.29^{\S\S\dagger}$ | $(37.98)^{\dagger\dagger}$ |
| *Maximum degree* | $755.18^{\S\S\S\dagger\dagger}$ | $(244.29)^{\dagger\dagger}$ |

$^{\S}$ Significantly different between young and aged with AD ($\S\ p < 0.05$, $\S\S\ p < 0.015$, $\S\S\S\ p < 0.001$).
$^{\dagger}$ Significantly different between aged and aged with AD ($\dagger\ p < 0.05$, $\dagger\dagger\ p < 0.015$, $\dagger\dagger\dagger\ p < 0.001$).

duced density in the aged with AD group is suggestive of reduced functional connectivity, related specifically to disease and not age alone, and closer analysis of one rather extreme case in the aged with AD group confirms the volatility of the disease on measures of functional connectivity.

## References


Achard, S., Salvador, R., Whitcher, B., Suckling, J., & Bullmore, E. (2006). A resilient, low-frequency, small-world human brain functional network with highly connected association cortical hubs. *J. Neurosci.*, **26**(1), 63–72.

Agata Fronczak, Piotr Fronczak, J. A. H. (2004). Average path length in random networks. *Physical Review E*, **70**, 056110.

Amaral, L. A. N., Scala, A., Barthelemy, M., & Stanley, H. E. (2000). Classes of Small World Networks. *Proceedings of the National Academy of Sciences*, **97**(21), 11149–11152.

Barabasi, A.-L. & Albert, R. (1999). Emergence of scaling in random networks. *Science*, **286**, 509–512.

Bassett, D. S. & Bullmore, E. (2006). Small-world brain networks. *Neuroscientist*, **12**(6), 512–23.

Beckmann, C. F. & Smith, S. M. (2004). Probabilistic Independent Component Analysis for Functional Magnetic Resonance Imaging. *IEEE Transactions on Medical Imaging*, **23**(2), 137–152.

Buckner, R. L., Snyder, A. Z., Sanders, A. L., Raichle, M. E., & Morris, J. C. (2000). Functional Brain Imaging of Young, Nondemented, and Demented Older Adults. *Journal of Cognitive Neuroscience*, **12**(Supplement 2), 24–34.

Buckner, R. L., Sepulcre, J., Talukdar, T., Krienen, F. M., Liu, H., Hedden, T., Andrews-Hanna, J. R., Sperling, R. A., & Johnson, K. A. (2009). Cortical hubs revealed by intrinsic functional connectivity: mapping, assessment of stability, and relation to Alzheimer's disease. *J. Neurosci.*, **29**(6), 1860–73.

Bullmore, E. & Sporns, O. (2009). Complex brain networks: graph theoretical analysis of structural and functional systems. *Nat. Rev. Neurosci.*, **10**(3), 186–98.

Buxton, R. B. (2009). *Introduction to Functional Magnetic Resonance Imaging: Principles and Techniques*. Cambridge University Press, Second edition.

Cox, R. W. (2011). AFNI: What a long strange trip it's been. *Neuroimage*, **In Press**.

Dale, A. M. & Buckner, R. L. (1997). Selective averaging of rapidly presented individual trials using fMRI. *Human Brain Mapping*, **5**(5), 329–340.

de Haan, W., Pijnenburg, Y. A. L., Strijers, R. L. M., van der Made, Y., van der Flier, W. M., Scheltens, P., & Stam, C. J. (2009). Functional neural network analysis in frontotemporal dementia and Alzheimer's disease using EEG and graph theory. *BMC Neurosci*, **10**, 101.

Diestel, R. (2005). *Graph Theory*. Springer-Verlag, 3rd edition.

Eguiluz, V. M., Chialvo, D. R., Cecchi, G. A., Baliki, M., & Apkarian, A. V. (2005). Scale-Free Brain Functional Networks. *Physical Review Letters*, **94**(1), 018102–1 – 018102–4e.

Filippi, M., editor (2009). *fMRI Techniques and Protocols*, volume 41 of *Neuromethods*. Humana Press.

Freeman, L. C. (1979). Centrality in Social Networks: Conceptual Clarification. *Social Networks*, **1**(3), 215–239.

Friston, K. J., Frith, C. D., Liddle, P. F., Dolan, R. J., Lammertsma, A. A., & Frackowiak, R. S. J. (1990). The Relationship Between Global and Local Changes in PET Scanas. *Journal of Cerebral Blood Flow and Metabolism*, **10**, 458–466.

Friston, K. J., Frith, C. D., Liddle, P. F., & Frackowiak, R. S. J. (1993). Functional Connectivity: The Principal-Component Analysis of Large (PET) Data Sets. *Journal of Cerebral Blood Flow and Metabolism*, **13**(1), 5–14.

Friston, K. J., Fletcher, P., Josephs, O., Holmes, A., Rugg, M. D., & Turner, R. (1998). Event-Related fMRI: Characterizing Differential Responses. *NeuroImage*, **7**(1), 30–40.

Gauthier, S., editor (2007). *Clinical Diagnosis and Management of Alzheimer's Disease*. Informa Healthcare, Third edition.

Greicius, M. D., Srivastava, G., Reiss, A. L., & Menon, V. (2004). Default-mode network activity distinguishes Alzheimer's disease from healthy aging: Evidence from functional MRI. *PNAS*, **101**(13), 4637–4642.

Hagmann, P., Kurant, M., Gigandet, X., Thiran, P., Wedeen, V. J., Meuli, R., & Thiran, J.-P. (2007). Mapping human whole-brain structural networks with diffusion MRI. *PLoS ONE*, **2**(7), e597.

He, Y., Chen, Z. J., & Evans, A. C. (2007). Small-world anatomical networks in the human brain revealed by cortical thickness from MRI. *Cereb. Cortex*, **17**(10), 2407–19.

He, Y., Chen, Z., & Evans, A. (2008). Structural insights into aberrant topological patterns of large-scale cortical networks in Alzheimer's disease. *J. Neurosci.*, **28**(18), 4756–66.

Humphries, M. D., Gurney, K., & Prescott, T. J. (2006). The brainstem reticular formation is a small-world, not scale-free, network. *Proc. Biol. Sci.*, **273**(1585), 503–11.

Leuchter, A. F., Newton, T. F., Cook, I. A., Walter, D. O., Rosenberg-Thompson, S., & Lachenbruch, P. A. (1992). Changes in Brain Functional Connectivity in Alzheimer-Type and Multi-Infarct Dementia. *Brain*, **115**(5), 1543–1561.

Mazziotta, J., Toga, A., Evans, A., Fox, P., Lancaster, J., Zilles, K., Woods, R., Paus, T., Simpson, G., Pike, B., Holmes, C., Collins, L., Thompson, P., MacDonald, D., Iacoboni, M., Schormann, T., Amunts, K., Palomero-Gallagher, N., Geyer, S., Parsons, L., Narr, K., Kabani, N., Le Goualher, G., Boomsma, D., Cannon, T., Kawashima, R., & Mazoyer, B. (2001). A probabilistic atlas and reference system for the human brain: International Consortium for Brain Mapping (ICBM). *Philos. Trans. R. Soc. Lond., B, Biol. Sci.*, **356**(1412), 1293–322.

Morris, J. C. (1997). Clinical Dementia Rating: A Reliable and Valid Diagnostic and Staging Measure for Dementia of the Alzheimer Type. *International Psychogeriatrics*, **9**(S1), 173–176.

Newman, M. E. J. (2002). Assortative mixing in networks. *Physical Review Letters*, **89**, 208701.

Newman, M. E. J. & Girvan, M. (2004). Finding and evaluating community structure in networks. *Physical Review E*, **69**, 026113.

Ogawa, S., Tank, D. W., Menon, R., Ellermann, J. M., Kim, S. G., Merkle, H., & Ugurbil, K. (1992). Intrinsic signal changes accompanying sensory stimulation: functional brain mapping with magnetic resonance imaging. *Proceedings of the National Academy of Sciences*, **89**(13), 5951–5955.

P. Erdős, A. R. (1960). On the evolution of random graphs. *Publications of the Mathematical Institute of the Hungarian Academy of Sciences*, **5**, 17–61.

Rodgers, J. L. & Nicewander, W. A. (1988). Thirteen Ways to Look at the Correlation Coefficient. *The American Statistician*, **42**(1), 59–66.

Rubinov, M. & Sporns, O. (2010). Complex network measures of brain connectivity: uses and interpretations. *Neuroimage*, **52**(3), 1059–69.

Shattuck, D. W. & Leahy, R. M. (2002). BrainSuite: An automated cortical surface identification tool. *Medical Image Analysis*, **6**(2), 129–142.

Shattuck, D. W., Sandor-Leahy, S. R., Schaper, K. A., Rottenberg, D. A., & Leahy, R. M. (2001). Magnetic Resonance Image Tissue Classification Using a Partial Volume Model. *NeuroImage*, **13**(5), 856–876.

Smith, S. M., Jenkinson, M., Woolrich, M. W., Beckmann, C. F., Behrens, T. E. J., Johansen-Berg, H., Bannister, P. R., De Luca, M., Drobnjak, I., Flitney, D. E., Niazy, R. K., Saunders, J., Vickers, J., Zhang, Y., De Stefano, N., Brady, J. M., & Matthews, P. M. (2004). Advances in functional and structural MR image analysis and implementation as FSL. *Neuroimage*, **23 Suppl 1**, S208–19.

Sorg, C., Riedl, V., Mühlau, M., Calhoun, V. D., Eichele, T., Läer, L., Drzezga, A., Förstl, H., Kurz, A., Zimmer, C., & Wohlschläger, A. M. (2007). Selective changes of resting-state networks in individuals at risk for Alzheimer's disease. *Proceedings of the National Academy of Sciences*, **104**(47), 18760–18765.

Sporns, O., Chialvo, D. R., Kaiser, M., & Hilgetag, C. C. (2004). Organization, development and function of complex brain networks. *Trends Cogn. Sci. (Regul. Ed.)*, **8**(9), 418–25.

Stam, C. J., Jones, B. F., Nolte, G., Breakspear, M., & Scheltens, P. (2007). Small-world networks and functional connectivity in Alzheimer's disease. *Cereb. Cortex*, **17**(1), 92–9.

Stam, C. J., de Haan, W., Daffertshofer, A., Jones, B. F., Manshanden, I., van Cappellen van Walsum, A. M., Montez, T., Verbunt, J. P. A., de Munck, J. C., van Dijk, B. W., Berendse, H. W., & Scheltens, P. (2009). Graph theoretical analysis of magnetoencephalographic functional connectivity in Alzheimer's disease. *Brain*, **132**(Pt 1), 213–24.

Strother, S. C. (2006). Evaluating fMRI Preprocessing Pipelines. *IEEE Engineering in Medicine and Biology Magazine*, **25**(2), 27–41.

Supekar, K., Menon, V., Rubin, D., Musen, M., & Greicius, M. D. (2008). Network analysis of intrinsic functional brain connectivity in Alzheimer's disease. *PLoS Comput. Biol.*, **4**(6), e1000100.

Ulmer, S. & Jansen, O., editors (2010). *fMRI: Basics and Clinical Applications*. Springer.

van den Heuvel, M. P., Stam, C. J., Kahn, R. S., & Hulshoff Pol, H. E. (2009). Efficiency of functional brain networks and intellectual performance. *J. Neurosci.*, **29**(23), 7619–24.

Vito Latora, M. M. (2001). Efficient Behavior of small-world networks. *Physical Review Letters*, **87**(19), 198701.

Wang, K., Liang, M., Wang, L., Tian, L., Zhang, X., Li, K., & Jiang, T. (2007). Altered functional connectivity in early Alzheimer's disease: a resting-state fMRI study. *Hum Brain Mapp*, **28**(10), 967–78.

Watts, D. J. & Strogatz, S. H. (1998). Collective dynamics of small-world networks. *Nature*, **393**, 440–442.

Woods, R., Cherry, S., & Mazziotta, J. (1992). Rapid automated algorithm for aligning and reslicing PET images. *Journal of Computer Assisted Tomography*, **16**(4), 620–633.